Design and Implementation of a Si_3N_4 Three-Stigmatic-Point Arrayed Waveguide Grating with a Resolving Power over 17,000

JIAHAO ZHAN,[1] YANG ZHANG,[1] WEI-LUN HSU,[1] SYLVAIN VEILLEUX,[2] MARIO DAGENAIS[1,*]

[1]*Department of Electrical and Computer Engineering, University of Maryland, College Park, MD 20770*
[2]*Department of Astronomy, University of Maryland, College Park, MD 20770*
[*]*dage@umd.edu*

Abstract: To provide a solution to the issue of the non-flat focal surface in traditional Rowland AWGs, we have designed and implemented a Si_3N_4 three-stigmatic-point arrayed waveguide grating (TSP AWG) with three inputs, and a spectral resolving power over 17,000 has been achieved experimentally. The flat focal surface of this AWG can accommodate a butt-coupled detector array positioned at the output facet without any reduction of the resolving power of the edge channels. Therefore, it is particularly advantageous to some astronomical applications which require an AWG as a light-dispersing component to obtain a complete 2D spectrum. As a proof-of-concept for next generation devices, the multi-input aspect of the design accommodates multiple single-mode fibers coming into the AWG. In addition, because the device is implemented on a high-index-contrast platform (Si_3N_4/SiO_2), a compact size of $\sim 9.3 \times 9.3$ mm^2 is achieved.

1. Introduction

The novel field of astrophotonics refers to the application of versatile photonic technologies to manipulate guided light collected from telescopes to achieve scientific goals in astronomy [1, 2]. It is widely believed to be a promising approach for solving some major challenges in observational astronomy, one of which is the miniaturization of the next-generation astronomical instrumentation [3]. Astronomers are building larger and larger telescopes, and in fact the next decade will mark the deployment of extremely-large telescopes (ELTs) with diameters (D) over 30 m [4]. As the size and cost of the associated conventional optical setups grow as D^2 - D^3, it will become much more challenging to maintain the stability of these giant optical systems. The key idea of astrophotonics is to collapse the bulk optics into 2D photonic integrated circuits to leverage the low-cost, compact, and robust nature of the integrated photonic platform [5–7].

One of the major scientific goals of the ELTs is to study the galaxies in the first billion years of the universe, which requires deep observations of faint sources and extract spectral information from the collected light. For this purpose, an integrated photonic spectrograph (IPS) has been proposed [8], which includes an arrayed waveguide grating (AWG) as the light-dispersing component. AWGs are widely used in modern telecommunication systems as multiplexers and signal routers [9]. As their main functionality is to spatially separate different wavelengths, they are well-suited for spectroscopic applications. The very first on-sky testing with an IPS obtained a spectrum of a type-S star which clearly captured the carbon monoxide molecular absorption features in the H band [10], and successfully demonstrated the possibility of obtaining meaningful astronomical spectra with an AWG.

However, each output channel of an AWG contains periodic pass frequencies from different spectral orders, spaced by the free spectral range (FSR). For astrophotonic spectroscopy applications, a complete spectrum is required and therefore, the overlapping spectral orders in each channel need to be separated by a secondary dispersion setup [11, 12]. A free space cross

disperser (e.g. a prism) is often employed to disperse the light in the perpendicular direction, and it is necessary to have the chip cleaved along the output focal plane of the AWG. However, this imposes a challenge on the traditional Rowland AWGs in which the focal surface is a circle. If the chip is cleaved along the tangent of the Rowland circle [Fig. 1(a)], the offset between the focal point and the cleaved facet will give rise to defocus aberrations for all channels except for the central one [Fig. 1(b)]. Thus, a flat focal plane is desired to minimize these defocus aberrations.

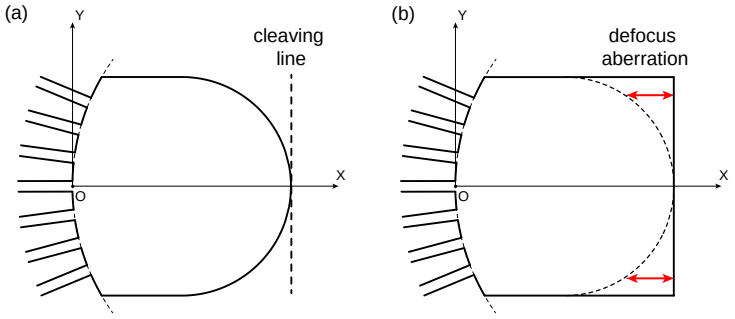

Fig. 1. (a) Mismatch between the circular focal plane and the straight cleaving line. (b) Defocus aberration induced by cleaving. The AWG with a rectangle output star coupler is referred to as a flat-Rowland AWG.

One solution is to incorporate a field-flattening lens on top of the output star coupler [13], which images the circular focal field into a flat one. However, this extra lens layer adds to the fabrication complexity significantly. Here we present a design and implementation of a Si_3N_4 three-stigmatic-point AWG (TSP AWG) based on the aberration theory proposed in [14, 15]. Different channels of a TSP AWG will inherently be focused onto a flat surface, and there is no reduction of the resolving power for the edge channels when the device is cleaved along the focal surface. The measured transmission spectrum of an implemented device shows a spectral resolving power of over 17,000. Note that when our TSP AWG was under development, A. Stoll et al. published their results of a similar device on a silica-on-silicon material platform [16]. In this work, we use a Si_3N_4/SiO_2 material platform, which has certain advantages. First, because of the larger index contrast, the waveguide bending radii can be reduced significantly, thus the device can be made much more compact in size. For astronomical applications, a more compact size means that the device is less sensitive to flexures, vibrations, and thermal drifts. Second, ultra-low propagation loss has been reported on Si_3N_4/SiO_2 material platforms of various thicknesses, which is critical for the photon-starved applications in astronomy. Another difference of this work from [16] is that we will demonstrate experimental results of a three-input TSP AWG. The multi-input aspect of this AWG is a proof-of-concept for next-generation devices, with more discussion given in Sec. 5.

2. Theory and Design

2.1. Brief summary of the aberration theory

A detailed description of the aberration theory is given in [14], and here we provide only a brief summary. Fig. 2 is a schematic illustration of an AWG, and its structure can be determined by three functions of w (w corresponds to the Y coordinate in Fig. 2, i.e., the distance along the Y axis) : (1) $u(w)$, which is the distance of the grating curve from the Y-axis in the X direction, (2) $L(w)$, which is the length of the array waveguide connecting a point $P(u, w)$ on the grating curve to the corresponding point $P'(u, w)$ at the output, and (3) $G(w)$, which is the number of array waveguides counted from the origin to the point $P(u, w)$. For the purpose of calculation,

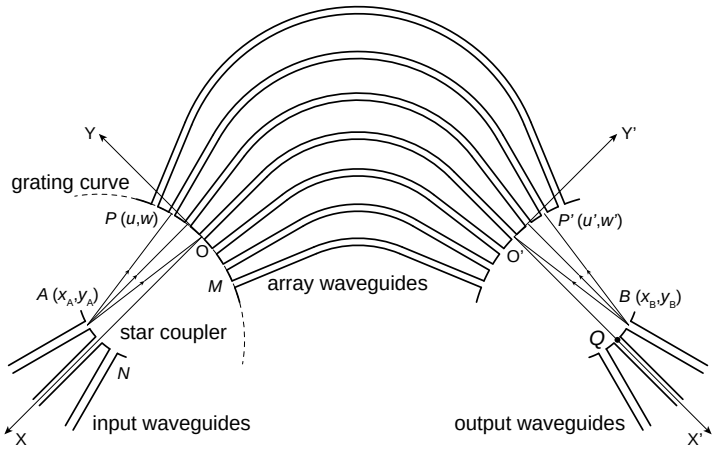

Fig. 2. Schematic illustration of an AWG consisting of I/O waveguides, input and output star couplers (FPRs) and an array of waveguides of different lengths.

$G(w)$ is allowed to be a continuous variable.

An optical path function (OPF) is defined to calculate the total path length from the input to one of the output channels:

$$F(w) = n_s\left[r_A(w) + r_B(w)\right] + n_w L(w) - G(w)m\lambda \tag{1}$$

where n_s and n_w are the effective indices of the star coupler and the array waveguides (they have slightly different values), m is the spectral order, $r_A(w)$ $[r_B(w)]$ is the geometric length between the input (output) channel and one of the array waveguides which includes the grating curve function $u(w)$. Note that $G(w)$ does not exist in real optical paths, but it is added such that the OPF is a constant for different values of w in an aberration-free system.

The OPF can also be expanded into a Taylor series

$$F(w) = F(0) + F'(0)w + \frac{1}{2}F''(0)w^2 + \cdots + \frac{1}{n!}F^{(n)}(0)w^n + \cdots \tag{2}$$

where

$$F^{(n)}(0) = n_s\left[r_A^{(n)}(0) + r_B^{(n)}(0)\right] + n_w L^{(n)}(0) - G^{(n)}(0)m\lambda \tag{3}$$

is the n^{th} aberration coefficient. $F^{(2)}(0)$, $F^{(3)}(0)$ and $F^{(4)}(0)$ correspond to the defocus, coma and spherical aberrations, respectively.

The key idea to flatten the circular focal surface of a Rowland AWG is to pick a series of collinear "stigmatic" points to define the flat focal surface. The fact that three functions can determine the structure of an AWG dictates that only three points $S_i (i = 1, 2, 3)$ can be included. By definition, all aberration coefficients vanish at these stigmatic points. Therefore, with Eq. (3) and the pre-chosen coordinates (x_i, y_i) and wavelengths (λ_i) of the stigmatic points, we have

$$n_s\left[r_A^{(n)}(0) + r_i^{(n)}(0)\right] + n_w L^{(n)}(0) - G^{(n)}(0)m\lambda_i = 0 \tag{4}$$

Eq. (4) can be solved in an iterative manner to extract the Taylor coefficients $u^{(n)}(0)$, $L^{(n)}(0)$, and $G^{(n)}(0)$, and then the structure of the TSP AWG can be determined.

2.2. Design of a low resolving power TSP AWG

As for the material platform, we use 100 nm-thick Si_3N_4 film, and the core of a single-mode waveguide has a width of 2 μm. The simulated TE mode profile is shown in Fig. 3, and the size of the mode (at $1/e^2$ width) is 3.6×2.9 μm^2. To maximize the coupling efficiency to a polarization-maintaining single-mode fiber, the waveguide width is tapered down to 600 nm at the edge of the chip to achieve the best mode matching. Our previous work has demonstrated a coupling efficiency of > 90% in the spectral range from 1450 to 1640 nm [17].

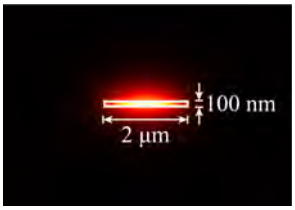

Fig. 3. Simulated TE mode of a waveguide core with dimensions of 2 μm by 100 nm.

As a proof-of-concept demonstration, we started with a TSP AWG of parameters listed in Table 1, targeting a low resolving power. The spectral resolving power R, defined by $\lambda/\Delta\lambda_{FWHM}$ (λ is center wavelength of the channel, and $\Delta\lambda_{FWHM}$ is the 3-dB width of the channel), is an important figure of merit to look for in the transmission spectrum of an AWG. The array waveguide spacing d_{ar} and I/O waveguide spacing d_{io} must be large enough to minimize the directional coupling between adjacent waveguides. Based on the waveguide geometry given in the last paragraph, our simulation shows that a spacing of 6 μm between the waveguides is enough to prevent the coupling between the waveguide modes. In addition, as the array waveguides fan out from the grating curve, the spacing between adjacent waveguides increases gradually, which further eliminates any possibility of mutual coupling.

Table 1. List of parameters of the proof-of-concept design.

Parameter	Explanation	Value
N_{in}	Number of input channels	1
N	Number of output channels	11
M	Number of array waveguides	35
λ_c	Center wavelength	1.55 μm
$\delta\lambda_{ch}$	Channel wavelength spacing	3 nm
W_{ar}	Array waveguide width	2 μm
d_{ar}	Array waveguide spacing	6 μm
d_{io}	I/O waveguide spacing	6 μm
R	Resolving Power	~ 960

First, the coordinates of the three stigmatic points are selected as $(R_o, 3d_{io})$, $(R_o, 0)$, and $(R_o, -3d_{io})$, corresponding to channel 3, 6 and 9, where R_o is the star coupler radius of the Rowland AWG with the same parameters as in Table 1. The value of R_o is extracted from our simulation software RSoft Photonics Suite. The wavelengths associated with these three stigmatic points are 1.541 μm, 1.55 μm, and 1.559 μm, respectively.

Next, $u(w)$, $L(w)$, and $G(w)$ are determined by solving Eq. (4) in an iterative manner. The calculated grating curve $u(w)$ is plotted as the blue dots in Fig. 4(a), and the grating curve of the corresponding Rowland AWG is plotted as the red curve for comparison. Fig. 4(b) shows the calculated extra length of the array waveguides $L_{ex}(w)$, which is determined by subtracting the length of the Rowland AWG array waveguides from the calculated length of the TSP AWG array waveguides. One can think of the $L_{ex}(w)$ term as a deviation from the "benchmark" value, which is the length of the array waveguides of the reference Rowland AWG. Here we notice three major structural differences in a TSP AWG compared to a Rowland AWG: (1) The grating curve is no longer a circle and it is defined by a polynomial function instead. (2) The length difference between adjacent waveguides in the array is no longer a constant, and an extra length is present. (3) The array waveguides are no longer uniformly distributed along the grating curve.

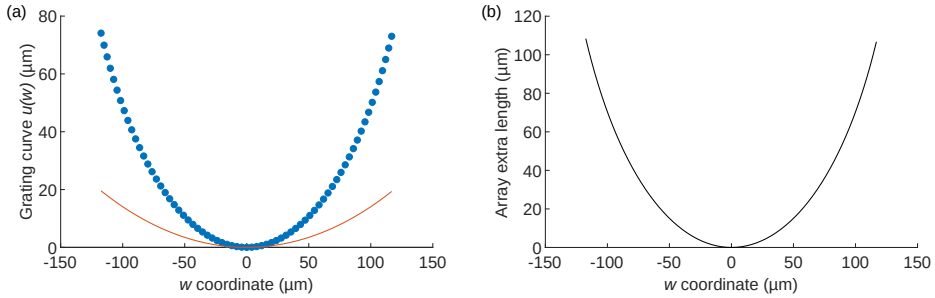

Fig. 4. (a) Calculated grating curve $u(w)$ of the designed TSP AWG (blue dotted), compared to the Rowland circle (red solid). (b) Extra length of the array waveguides of the designed TSP AWG.

Finally, the layout design of the TSP AWG must be completed, and the extra length term $L_{ex}(w)$ needs to be incorporated into the array waveguides. As for Rowland AWGs, it is well known that the length difference ΔL between adjacent waveguides is given by $\Delta L = m\lambda_c/n_w$. Each array waveguide comprises three segments: one straight waveguide of length zL_i, one arc of radius zR_i and angle $2\theta_i$ (in degree), and another straight waveguide identical with the first one, as depicted in Fig. 5(a). Half of the spacing between the two star couplers is denoted by L_g, which determines the minimum bending radius in the array waveguides. R_{end} is the distance from the input waveguide to the starting point of one of the array waveguides. In the case of a Rowland AWG, it is a constant equal to the radius of the Rowland circle.

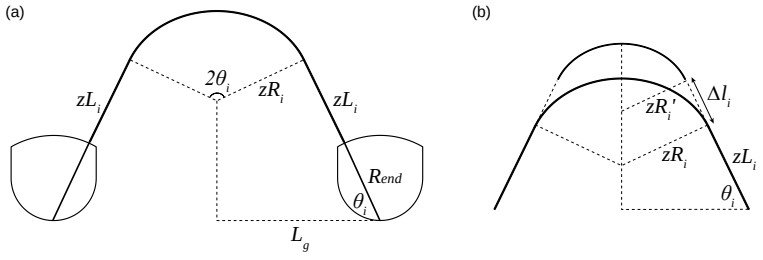

Fig. 5. (a) Array waveguide layout and key parameters in Rowland AWGs. (b) Extending the straight segment to account for the extra length in each array waveguide in TSP AWGs.

Since the length difference between adjacent waveguides is equal to ΔL, the following system of equations can be derived:

$$
\begin{aligned}
zR_i \sin\theta_i + (R_{end} + zL_i)\cos\theta_i &= L_g \\
zR_i P\theta_i - zR_1 P\theta_1 + zL_i - zL_1 &= \tfrac{i-1}{2}\Delta L
\end{aligned}
\tag{5}
$$

where $P = \pi/180$. Given the values of ΔL and L_g, Eq. (5) can be solved to obtain zL_i and zR_i, and the layout of the array waveguides is determined.

As for TSP AWGs, there are two main differences: (1) R_{end} is no longer a constant for different channels, since the star coupler is no longer defined by an arc. (2) There is an extra length $L_{ex,i}$ associated with each array waveguide. For (1), R_{end} of each channel can be numerically calculated (denoted by rAr_i), once the grating curve function $u(w)$ is obtained. Fig. 5(b) demonstrates how the extra length is incorporated in the layout - via the extension of the straight section with an amount of Δl_i. From some basic geometry, the following system of equations can be derived:

$$
\begin{aligned}
L_i &= 2(rAr_i + zL_i + zR_i P\theta_i) \\
L_i' &= 2(rAr_i + zL_i + \Delta l_i + zR_i' P\theta_i) \\
zR_i' &= zR_i - \Delta l_i/\tan\theta_i \\
L_i' - L_i &= L_{ex,i}
\end{aligned}
\tag{6}
$$

where L_i and L_i' are the lengths of the array waveguide before and after the extension of the straight segment, respectively, and the difference between the two is equal to the extra length $L_{ex,i}$. Solving for Δl_i and zR_i', the layout of the array waveguides for TSP AWGs can be determined.

3. Simulation and experimental results

3.1. Device simulation

A direct modeling of the TSP AWG in RSoft is difficult, as the built-in AWG simulation utility supports only the Rowland structures. The general simulation flow in RSoft is: First, a BPM (Beam-Propagation Method) simulation is performed on the input star coupler, to obtain the power and initial phase distribution of the array waveguides. Next, the phase is evolved based on the length of the array waveguides. Then the power and updated phase are combined into an electric field profile, which will be injected into the output star coupler. Finally the emerging optical power from the output waveguides are recorded and a complete spectrum can be obtained by repeating the above steps for all wavelengths.

With the same idea in mind, we have developed the following simulation flow for TSP AWGs: (1) In RSoft, modify the geometry of the input star coupler based on the calculated grating curve $u(w)$, and perform BPM simulation to obtain inital power and phase information. (2) Modify the output star coupler similarly, and add launch fields for each array waveguide. Optical modes will be launched into the output star coupler via these launch fields, and the output power from each channel will be monitored. (3) Use a custom-developed routine to calculate the phase based on the length of the array waveguides and create launch field data files for each wavelength. The entire simulation process is also controlled by this routine.

The simulated transmission spectra of the designed TSP AWG with parameters listed in Table 1 and the corresponding Rowland AWG are plotted in Fig. 6(a) and (c), respectively. Fig. 6(b) and (d) are the calculated resolving powers of the two AWGs with error bars included. The uncertainty comes from the inaccuracy in the measured 3-dB width of each channel because of the chosen wavelength step during spectrum simulation, as a compromise for reduced simulation time. Since N discrete waveguides are placed on the output focal surface to guide the N output channels, theoretically a well-designed TSP AWG should demonstrate a similar spectral resolving

power compared to the corresponding Rowland AWG. And this is indeed the case comparing Fig. 6(b) and 6(d), which implies that the circular focal surface has been flattened in the TSP AWG.

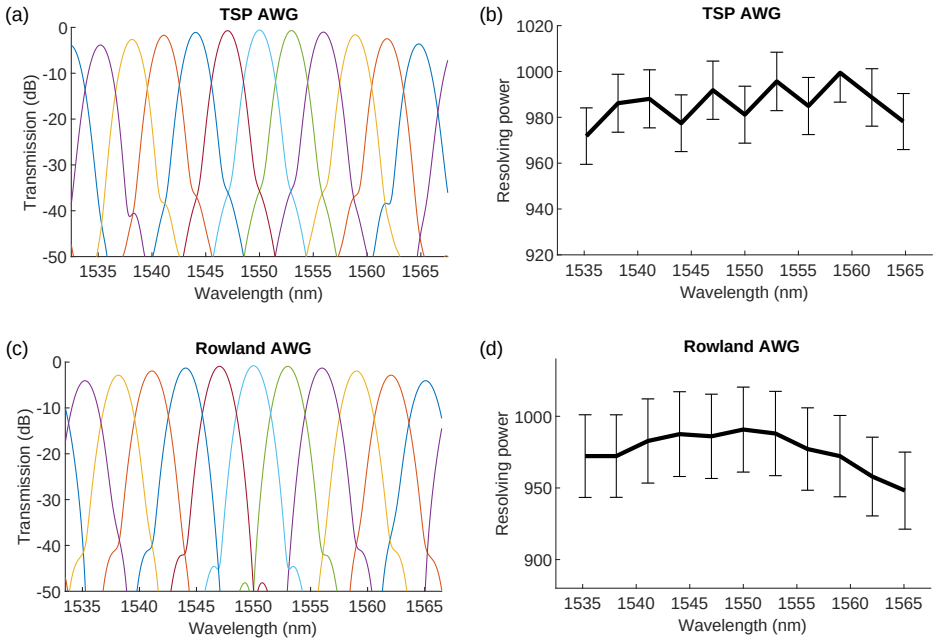

Fig. 6. (a) Simulated transmission spectra and (b) resolving power of the designed TSP AWG. (c) Simulated transmission spectra and (d) resolving power of the corresponding Rowland AWG, with error bars included.

3.2. Device fabrication and characterization

To better compare the device performances, both the designed TSP AWG and the corresponding Rowland AWG are fabricated with the following procedures.

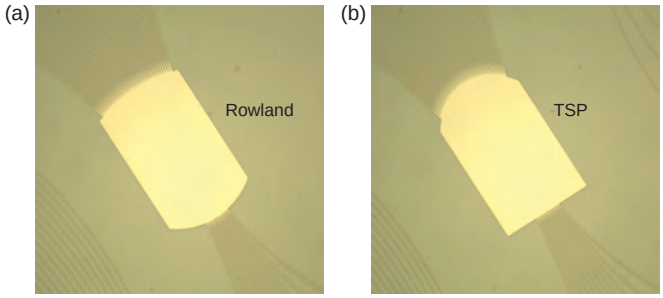

Fig. 7. Optical microscope images of the output star couplers of (a) the Rowland AWG and (b) the TSP AWG. The light enters from the array waveguides at the top, and exits from the output channel waveguides at the bottom.

First, a thin layer (100 nm) of stoichiometric Si_3N_4 is deposited via low-pressure chemical vapor deposition (LPCVD) on a silicon wafer with 10-μm thermal SiO_2 on top. Device patterning is performed by e-beam lithography followed by a developing process to remove the exposed resist. Next, chromium ($\sim$ 20 nm) is deposited as a hard mask, and then the patterns are

transferred into the Si_3N_4 layer by a CHF_3/O_2-based plasma etching process. After the removal of the Cr hard mask, a top SiO_2 cladding layer is deposited via plasma-enhanced chemical vapor deposition (PECVD). Following these fabrication procedures, we are able to achieve an ultra-low propagation loss of 0.018 dB/cm [18], which is critical for the photon-starved applications in astronomy. Optical microscope images of these fabricated Rowland and TSP AWGs are shown in Fig. 7, in which the structural differences between the two star couplers are clearly demonstrated: the grating curve of the TSP AWG has a larger curvature, and the focal surface is flat.

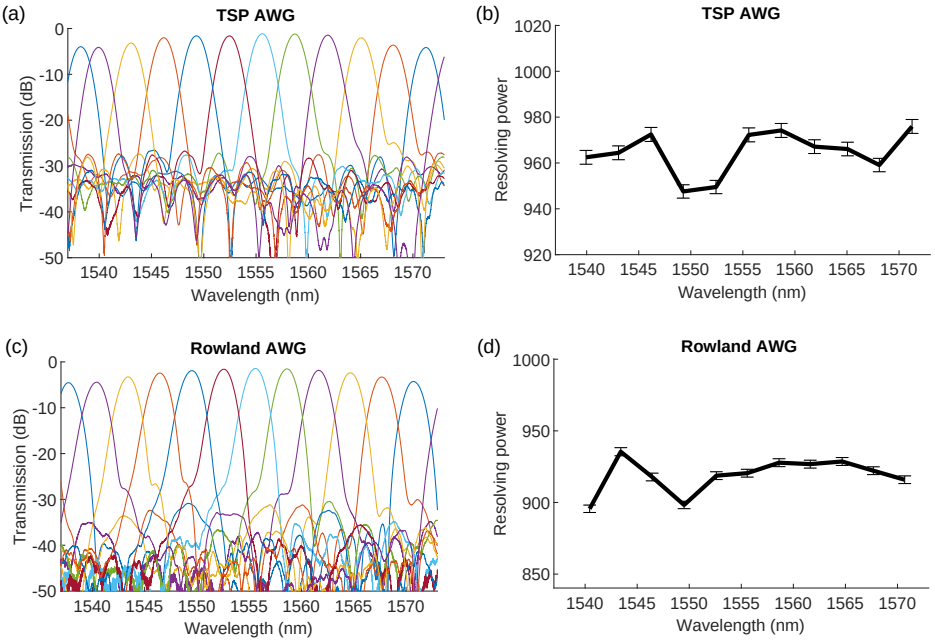

Fig. 8. (a) Measured transmission spectra and (b) calculated resolving power of the designed TSP AWG. (c) Measured transmission spectra and (d) calculated resolving power of the corresponding Rowland AWG, with error bars included.

The measured transmission spectra of the fabricated AWGs and the corresponding spectral resolving power are plotted in Fig. 8. Note that the error bars are much less than those in Fig. 6, since the wavelength sweep was performed with a finer resolution. For both AWGs, a good agreement between the experimental and simulated results is achieved. The on-chip loss of both fabricated devices (measured relative to the reference waveguide) is ~ -1.5 dB for the center channel, the side lobes are more than 25 dB down, and the measured resolving power is similar to that in the simulation.

4. Demonstration of a TSP AWG with a large resolving power

For practical applications such as astronomical spectroscopy, TSP AWGs with larger resolving powers must be implemented. As the above proof-of-concept design works as expected, the same structure and layout design procedures can be applied. We have designed another TSP AWG with parameters listed in Table 2. Other parameters not listed are the same as in Table 1. The dimensions of this designed TSP AWG are $\sim 9.3 \times 9.3$ mm^2, excluding the I/O waveguides.

In this case, three input channels are included, which is to accommodate multiple single-mode fibers coming into the AWG. This is a critical feature to have for the integrated spectrograph application, in which the light at the telescope focal plane is first coupled into a multi-mode fiber, then a so-called “photonic lantern” device [19] adiabatically converts the multi-mode core into

Table 2. List of parameters of the other two TSP AWGs with higher resolving powers.

Parameter	N_{in}	N	M	$\delta\lambda_{ch}$ (nm)	R
Value	3	101	201	0.15	~ 17,000

several single-mode cores. A complete layout diagram of the designed TSP AWG along with three microscopic images of a fabricated device are shown in Fig. 9.

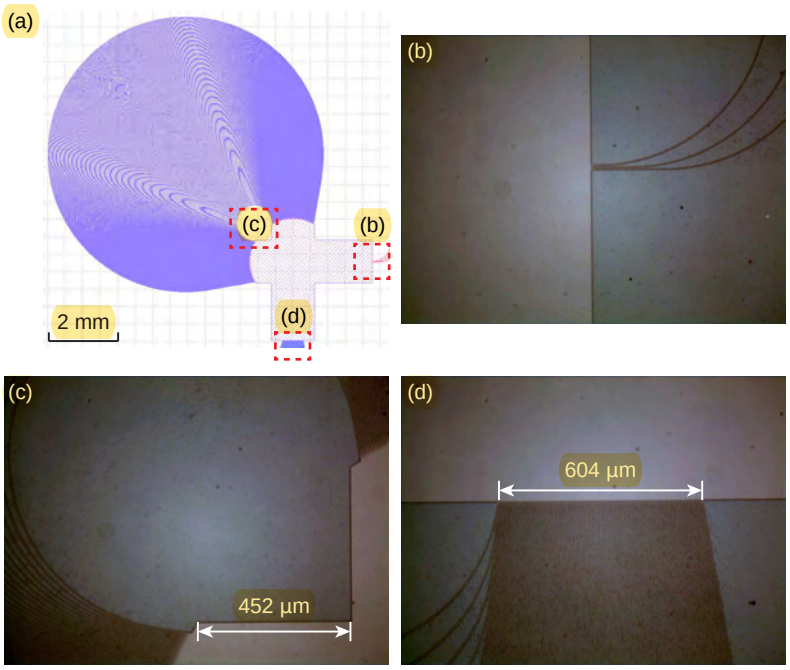

Fig. 9. (a) Layout diagram of the designed TSP AWG. (b), (c), and (d) are the corresponding optical microscope images of the three regions marked by the red dashed rectangle in (a).

Fig. 10 shows the measurement results of the fabricated device. (a), (c), and (e) correspond to the transmission spectra measured with the center input channel and the two edge input channels, respectively. Note that for clarity, only 21 output channels (1 in 5) are plotted in the spectra. However, the resolving power plots (b), (d), and (f) have all output channels included. The complete transmission spectra for all three input channels are provided in the supplemental document. From Fig. 10, it is shown that the on-chip loss of the fabricated device (measured relative to the reference waveguide) is ~ -2 dB for the center channel, the side lobes are ~ 15 dB down, and the noise floor is slightly higher than the results in Fig. 8. To calculate the resolving power of each channel, the 3-dB width is extracted by finding the two adjacent data points on each side of the peak, and then performing a linear interpolation. A resolving power of over 17,000 is achieved for all three input channels.

As TSP AWG is prone to chromatic defocus [16], here we have also investigated the full spectrum of our designed TSP AWG in the spectral range from 1450 nm to 1640 nm, and the results are plotted in Fig. 11. We can see that the fabricated device still suffers from chromatic dispersion, however, the variation of the resolving power is ~ 2k (ignoring the outliers).

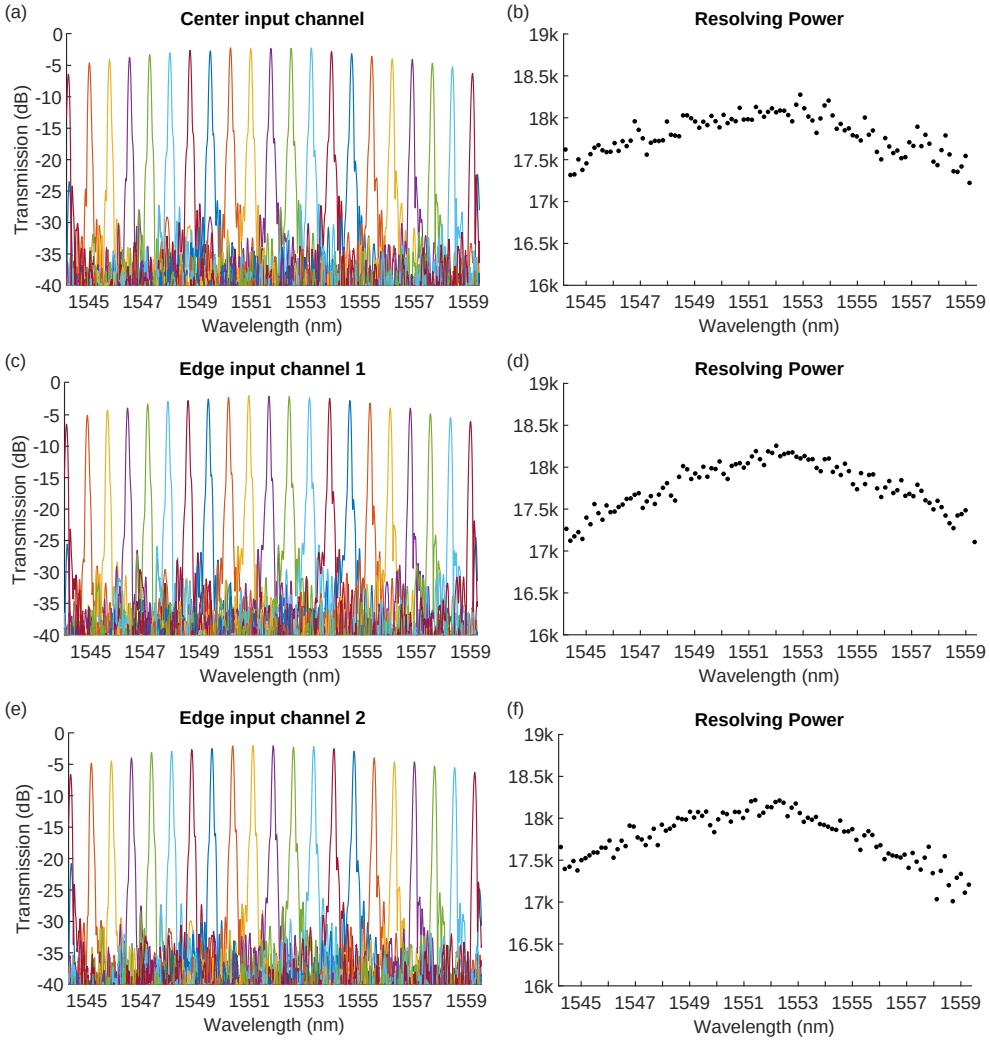

Fig. 10. (a) Measured transmission spectra and (b) calculated resolving power of the large-R TSP AWG, with the input light from the center channel. (c) Measured transmission spectra and (d) calculated resolving power of the large-R TSP AWG, with the input light from one of the edge channels. (e) Measured transmission spectra and (f) calculated resolving power of the large-R TSP AWG, with the input light from the other edge channel. For clarity, only a total of 21 channels are plotted in the transmission spectra. The resolving power plots have all channels included.

Comparing to the theoretical prediction of the same layout shown in [16], the variation is $\sim$ 10k. This indicates that using a compact Si_3N_4 platform helps reduce chromatic defocus.

5. Conclusion and Outlook

We have presented the design and implementation of a Si_3N_4 three-stigmatic-point AWG, with a detailed discussion of the layout design and simulation method. A spectral resolving power of over 17,000 has been achieved experimentally. Thanks to the flat focal surface of the TSP AWG, the defocus aberration of the edge channels is minimized, thus improving the resolving power at

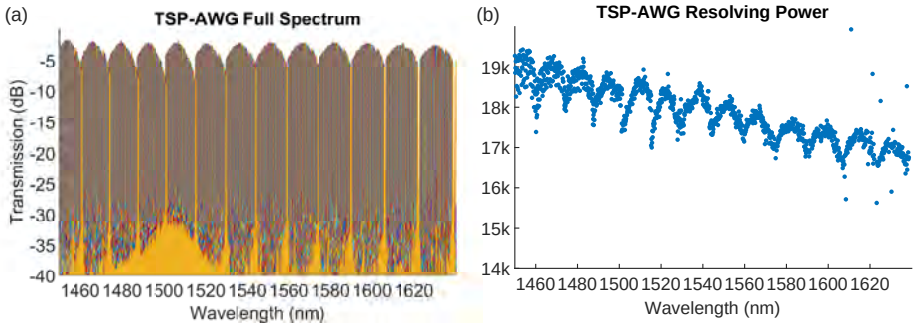

Fig. 11. (a) Complete transmission spectrum of the designed TSP AWG from 1450 nm to 1640 nm. (b) Calculated resolving power of all the transmission peaks in (a).

the same time. This design provides a solution for a flat-focal-field spectrometer, fulfilling the requirement of an integrated astronomical spectrograph in which the chip needs to be cleaved along the output focal surface to accommodate a linear detector array.

As we have mentioned in the last section, a "few-input" AWG is desired in astronomical spectroscopy applications to interface with a photonic lantern. In the future, we intend to have as many as 7 closely spaced input waveguides so that the output spectra from the input waveguides lie on top of each other to within 2-4 pixels on the detector array, effectively recombining the light split by 1×7 photonic lanterns while still delivering an effective spectral resolution that is sufficient to map the internal motions of faint distant galaxies ($\sim$ 100 km/s or R $\sim$ 3000). This translates into a huge gain in sensitivity compared with current instruments, where the spectra from the input SMFs are never recombined and the read-out noise of the detector is the limiting factor at faint flux levels.

Another important consideration is the polarization diversity, as light collected from the universe is unpolarized in nature. It will be highly advantageous if the integrated photonic spectrograph can handle both polarizations, when the number of available photons are already quite limited. A polarization-independent Rowland AWG has been demonstrated by having two inputs for the two polarizations [20]. For TSP AWGs, a possible solution for including polarization diversity is to first separate the two polarizations with a large-bandwidth polarization beam splitter [21], and then handle the two polarizations with two customized TSP AWGs.

Funding. National Science Foundation (NSF) under grant 1711377 and the National Aeronautics and Space Administration (NASA) under grant 16-APRA 16-0064.

Acknowledgments. We thank Dr. Yi-Wen Hu for the initial development of the MATLAB routine for the demonstration of the aberration theory, and Dr. Pradip Gatkine for helpful discussions. We thank the reviewers for their constructive comments and suggestions which improved this manuscript.

Disclosures. The authors declare no conflicts of interest.

Data Availability. Data underlying the results presented in this paper are not publicly available at this time but may be obtained from the authors upon reasonable request.

Supplemental document. See Supplement 1 for supporting content.

References

1. N. K. Pervez, W. Cheng, Z. Jia, M. P. Cox, H. M. Edrees, and I. Kymissis, "Photonic crystal spectrometer," Opt. Express **18**, 8277–8285 (2010).
2. G. Roelkens, U. Dave, A. Gassenq, N. Hattasan, C. Hu, B. Kuyken, F. Leo, A. Malik, M. Muneeb, E. Ryckeboer, S. Uvin, Z. Hens, R. Baets, Y. Shimura, F. Gencarelli, B. Vincent, R. Loo, J. V. Campenhout, L. Cerutti, J.-B. Rodriguez, E. Tournié, X. Chen, M. Nedeljkovic, G. Mashanovich, L. Shen, N. Healy, A. C. Peacock, X. Liu,

R. Osgood, and W. Green, "Silicon-based heterogeneous photonic integrated circuits for the mid-infrared," Opt. Mater. Express **3**, 1523–1536 (2013).
3. R. J. Harris and J. R. Allington-Smith, "Applications of integrated photonic spectrographs in astronomy," Mon. Notices Royal Astron. Soc. **428**, 3139–3150 (2012).
4. J. Bland-Hawthorn and P. Kern, "Astrophotonics: a new era for astronomical instruments," Opt. Express **17**, 1880–1884 (2009).
5. K. Chaganti, I. Salakhutdinov, I. Avrutsky, and G. W. Auner, "A simple miniature optical spectrometer with a planar waveguide grating coupler in combination with a plano-convex lens," Opt. Express **14**, 4064–4072 (2006).
6. J. Allington-Smith and J. Bland-Hawthorn, "Astrophotonic spectroscopy: defining the potential advantage," Mon. Notices Royal Astron. Soc. **404**, 232–238 (2010).
7. A. Z. Subramanian, E. Ryckeboer, A. Dhakal, F. Peyskens, A. Malik, B. Kuyken, H. Zhao, S. Pathak, A. Ruocco, A. D. Groote, P. Wuytens, D. Martens, F. Leo, W. Xie, U. D. Dave, M. Muneeb, P. V. Dorpe, J. V. Campenhout, W. Bogaerts, P. Bienstman, N. L. Thomas, D. V. Thourhout, Z. Hens, G. Roelkens, and R. Baets, "Silicon and silicon nitride photonic circuits for spectroscopic sensing on-a-chip [invited]," Photon. Res. **3**, B47–B59 (2015).
8. P. Gatkine, S. Veilleux, and M. Dagenais, "Astrophotonic spectrographs," Appl. Sci. **9** (2019).
9. S. Pathak, P. Dumon, D. Van Thourhout, and W. Bogaerts, "Comparison of AWGs and Echelle gratings for wavelength division multiplexing on silicon-on-insulator," IEEE Photonics J. **6**, 1–9 (2014).
10. Cvetojevic, N., Jovanovic, N., Betters, C., Lawrence, J. S., Ellis, S. C., Robertson, G., and Bland-Hawthorn, J., "First starlight spectrum captured using an integrated photonic micro-spectrograph," AA **544**, L1 (2012).
11. R. G. Tull, P. J. MacQueen, C. Sneden, and D. L. Lambert, "The high-resolution cross-dispersed Echelle white-pupil spectrometer of the McDonald Observatory 2.7-m telescope," Publ. Astron. Soc. Pac. **107**, 251 (1995).
12. Y.-W. Hu, "Ultra-low-loss silicon nitride waveguide gratings and their applications in astrophotonics," Ph.D. thesis, University of Maryland, College Park (2020).
13. B. I. Akca, G. Sengo, M. Pollnau, A. Driessen, K. Wörhoff, and R. M. de Ridder, "Flat-focal-field integrated spectrometer using a field-flattening lens," Opt. Lett. **37**, 4281–4283 (2012).
14. D. Wang, G. Jin, Y. Yan, and M. Wu, "Aberration theory of arrayed waveguide grating," J. Light. Technol. **19**, 279–284 (2001).
15. S. Lu, C. Yang, Y. Yan, G. Jin, Z. Zhou, W. H. Wong, and E. Y. B. Pun, "Design and fabrication of a polymeric flat focal field arrayed waveguide grating," Opt. Express **13**, 9982–9994 (2005).
16. A. Stoll, K. Madhav, and M. Roth, "Design, simulation and characterization of integrated photonic spectrographs for astronomy II: low-aberration generation-II AWG devices with three stigmatic points," Opt. Express **29**, 36226–36241 (2021).
17. T. Zhu, Y. Hu, P. Gatkine, S. Veilleux, J. Bland-Hawthorn, and M. Dagenais, "Ultrabroadband high coupling efficiency fiber-to-waveguide coupler using Si_3N_4/SiO_2 waveguides on silicon," IEEE Photonics J. **8**, 1–12 (2016).
18. Y. Zhang, J. Zhan, S. Veilleux, and M. Dagenais, "Silicon nitride Fabry-Perot Bragg grating nanoresonator with ultrahigh intrinsic Q," in *Conference on Lasers and Electro-Optics,* (Optica Publishing Group, 2022), p. SM4G.7.
19. S. G. Leon-Saval, A. Argyros, and J. Bland-Hawthorn, "Photonic lanterns: a study of light propagation in multimode to single-mode converters," Opt. Express **18**, 8430–8439 (2010).
20. Q. Han, J. St-Yves, Y. Chen, M. Ménard, and W. Shi, "Polarization-insensitive silicon nitride arrayed waveguide grating," Opt. Lett. **44**, 3976–3979 (2019).
21. J. Zhan, M. Dagenais, G. Yang, and S. Veilleux, "A broadband Si_3N_4 polarization beam splitter based on asymmetric directional couplers," in *2021 Photonics North (PN),* (2021), pp. 1–1.